RNA (1997), 3:561–576. Cambridge University Press. Printed in the USA.

Analysis of the tertiary structure of the ribonuclease P ribozyme–substrate complex by site-specific photoaffinity crosslinking

MICHAEL E. HARRIS,[1] ALEXEI V. KAZANTSEV,[2] JIUNN-LIANG CHEN,[2] and NORMAN R. PACE[2]

[1]Department of Molecular Biology and Microbiology, School of Medicine, Case Western Reserve University, Cleveland, Ohio 44106-4960, USA
[2]Department of Plant and Microbial Biology and Department of Molecular and Cell Biology, University of California, Berkeley, California 94720-3102, USA

ABSTRACT

Bacterial ribonuclease P (RNase P), an endonuclease involved in tRNA maturation, is a ribonucleoprotein containing a catalytic RNA. The secondary structure of this ribozyme is well-established, and a low-resolution model of the three-dimensional structure of the ribozyme–substrate complex has been proposed based on site-specific crosslinking and phylogenetic comparative data [Harris ME et al., 1994 *EMBO J 13*:3953–3963]. However, several substructures of that model were poorly constrained by the available data. In the present analysis, additional constraints between elements within the *Escherichia coli* RNase P RNA-pre-tRNA complex were determined by intra- and intermolecular crosslinking experiments. Circularly permuted RNase P RNAs were used to position an azidophenacyl photoactive crosslinking agent specifically at strategic sites within the ribozyme–substrate complex. Crosslink sites were mapped by primer extension and confirmed by analysis of the mobility of the crosslinked RNA lariats on denaturing acrylamide gels relative to circular and linear RNA standards. Crosslinked species generally retained significant catalytic activity, indicating that the results reflect the native ribozyme structure. The crosslinking results support the general configuration of the structure model and predicate new positions and orientations for helices that were previously poorly constrained by the data set. The expanded library of crosslinking constraints was used, together with secondary and tertiary structure identified by phylogenetic sequence comparisons, to refine significantly the model of RNase P RNA with bound substrate pre-tRNA. The crosslinking results and data from chemical-modification and mutational studies are discussed in the context of the current structural perspective on this ribozyme.

Keywords: ribozyme; RNA structure; crosslinking; ribonuclease P; tRNA

INTRODUCTION

Ribonuclease P (RNase P) catalyzes the hydrolysis of a specific phosphodiester bond in pre-tRNA to generate the 5′ end of mature tRNA. RNase P enzymes are found in members of all three phylogenetic domains, and all of the cellular RNase P enzymes characterized to date have essential RNA subunits (e.g., Guerrier-Takada et al., 1983; Cherayil et al., 1987; LaGrandeur et al., 1993). A convincing alignment of the RNase P RNA sequences from representatives of all three phylogenetic domains has not yet been achieved, but sequence and structural similarities are clear (see Chen & Pace in this issue). Thus, bacterial, archaeal, and eucaryal RNase P RNAs are "homologous," that is, they share ancestry. In Bacteria, the RNase P holoenzyme is a heterodimer composed of single protein (ca. 120 amino acids) and RNA (ca. 400 nt) components. Under in vitro reaction conditions of high ionic strength and in the presence of required divalent metal ions, bacterial RNase P RNAs retain the substrate-binding and catalytic properties of the holoenzyme, and so constitute one class of large ribozymes (Guerrier-Takada et al., 1983; for recent comparison of large ribozymes, see Cech, 1993). The ubiquitous occurrence of RNase P as a ribonucleoprotein and the catalytic nature of the bacterial RNA implies an ancient and important role for RNA in the function of this enzyme. Understanding the role that the RNA plays in the function of RNase P requires knowledge of its structure.

Reprint requests to: Norman R. Pace, Department of Plant and Microbial Biology, 111 Koshland Hall, University of California, Berkeley, California 94720-3102, USA; e-mail: nrpace@nature.berkeley.edu.

The secondary structure of the bacterial RNase P RNA is now well-established by phylogenetic sequence comparisons (James et al., 1988; Haas et al., 1997). Sequence comparisons identify a subset of helices, termed core helices, that are present in all bacterial RNase P RNAs and so are likely to be important in the function of the ribozyme. In addition, there are regions of the core structure that, in different organisms, often contain nonconserved structural elements. These elements also often are subject to substantial variation in sequence-length, suggesting that they are located on the periphery of the common, core tertiary structure. Sequence comparisons also identify phylogenetically conserved nucleotides, which, therefore, presumably are particularly important for structure or function. Nucleotides that are invariant among all known bacterial RNase P RNAs are distributed throughout the core of the secondary structure model. It is imagined that the active site of the ribozyme is composed of multiple conserved functional groups that are located in separate regions of the RNA chain and brought together in the three-dimensional structure.

Mutational (e.g., Shiraishi & Shimura, 1986; Baer et al., 1988; Kirsebom & Svärd, 1993; Schlegl et al., 1994) and crosslinking (Burgin & Pace, 1990) studies have indicated some regions of the RNA that probably are involved in catalysis. Additionally, specific residues within the ribozyme that are important for catalytic function have been identified (Harris & Pace, 1995), however, the structural details of the active site remain undetermined. A few sites of contact between the ribozyme and its substrate were established recently (Kirsebom & Svärd, 1994; Oh & Pace, 1994; Pan et al., 1995) and some long-range intramolecular interactions that may act to stabilize the ribozyme's structure have been proposed (Brown et al., 1996). Nonetheless, our perception of the three-dimensional structure of the RNase P ribozyme–substrate complex has been rudimentary.

The crystal structures of the hammerhead ribozyme (Pley et al., 1994; Scott et al., 1995) and particularly the P4–6 domain of GI introns (Cate et al., 1996) provide a detailed view of the complexity of RNA folding. We expect the general features of these models and many of the specific structure motifs, as well, to be directly applicable to RNase P structure. These include tight packing of RNA helices, long-range tertiary interactions and regions of non-Watson–Crick pairing at complex helix junctions. At present, we have only very limited insight into the kind and number of these interactions in RNase P RNA. In addition to crystal structures of RNAs described above, theoretical models, such as those available for the 16S ribosomal subunit (Brimacombe, 1995; Stern et al., 1988; Malhotra & Harvey, 1994) and the catalytic core of the GI ribozyme (Michel & Westhof, 1990), are useful tools for designing experiments and interpreting structural data. Two recent efforts at modeling RNase P RNA structure have been reported (Harris et al., 1994; Westhof et al., 1996). Additional structural constraints are required to test the usefulness of these structure models and improve perspective on RNase P RNA conformation.

One experimental method for obtaining information bearing on the tertiary structure of RNA chains is chemical crosslinking to establish proximal regions within or between molecules. We have used circularly permuted tRNAs and RNase P RNAs (cpRNAs) to attach photoactivatable crosslinking agents at several strategic sites in the ribozyme–substrate complex in order to investigate its global architecture (Nolan et al., 1993; Harris et al., 1994). cpRNAs retain the native RNA sequence, but the native 5′ and 3′ ends are joined by a short oligonucleotide linker, and novel termini are located elsewhere in the structure. Such constructs permit the specific attachment of chemical reagents to nucleotides that normally are on the interior of RNA sequences with the specificity and efficiency of end modification.

In the present analysis, our low-resolution structure model (Harris et al., 1994) has been refined substantially using results from additional site-specific photoaffinity crosslinking experiments. Six novel photoagent attachment sites were analyzed in order to gain perspective on the position and orientation of core helices that were poorly constrained in the previous crosslinking and modeling study. The crosslinked RNAs generally retained full catalytic activity, indicating that the crosslinking results are relevant to the native structure of the ribozyme. The expanded body of crosslinking results, together with secondary and tertiary structure identified by phylogenetic sequence comparisons, and recent experimental data bearing on specific contacts within the ribozyme–substrate complex, are used to refine significantly the model of the structure of the RNase P ribozyme–substrate complex.

RESULTS

Photoaffinity crosslinking using circularly permuted RNase P RNAs

The secondary structure of *Escherichia coli* RNase P RNA is shown in Figure 1. In the present analysis, specific photoagent attachment sites were developed to provide information bearing on regions of the structure that were poorly constrained by previously available data. The locations of the new endpoints in the circularly permuted RNase P RNAs used in this analysis were selected primarily due to their strategic positions in the structure model; however, the use of phage T7 RNA polymerase for in vitro transcription dictated that the RNAs initiate with a guanosine residue (Milligan & Uhlenbeck, 1989). Three of the sites chosen are located within helices already constrained by the avail-

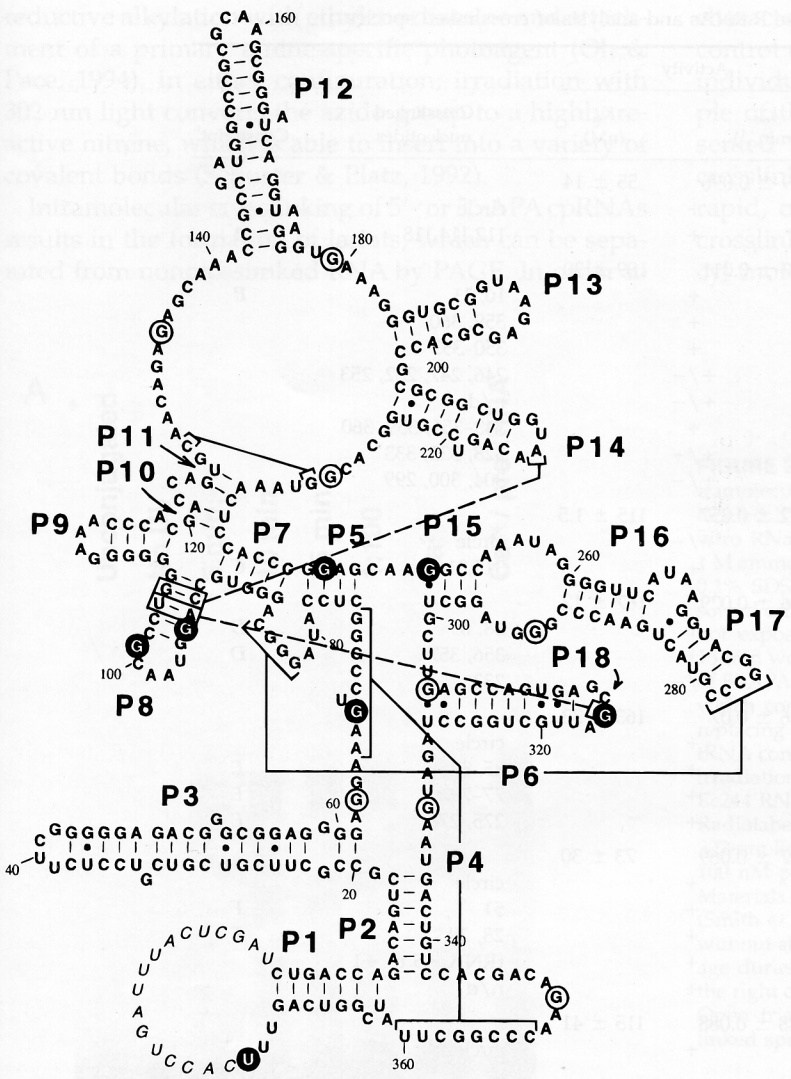

FIGURE 1. Locations of photoagent attachment sites. The secondary structure of *E. coli* RNase P RNA is shown with photoagent attachment sites circled. Sites described in this study are indicated by filled circles, and attachment sites described previously (Harris et al., 1994) are shown as open circles. The numbering of RNase P RNA is that of the native sequence. Non-native nucleotides included in the circularly permuted RNase P RNAs are italicized. Three pairing interactions in the *E. coli* secondary structure (P4, P6, and G230-C128) are indicated by brackets connected by lines. Tertiary interactions identified by covariation analysis (Brown et al., 1996) involving the GNRA tetraloops of P14 and P18 are indicated by dashed lines. The nomenclature used in describing the secondary structure is modeled after that of Group I introns (Burke et al., 1987), as described (Haas et al., 1994). Helices are numbered as they occur 5′ to 3′, preceded by the designation P (paired; e.g., P3 is the third helix from the 5′ end). The loops of individual helices are numbered as the helix with which they are associated, with the prefix L (loop; e.g., L3 is the loop associated with P3). Sequences between helices are numbered with the helices they connect, with the prefix J (joining; e.g., J3/4 is the sequence linking P3 and P4).

able crosslinking data (Ec68 in P4, Ec244 in P5, and Ec250 in P15; Fig. 1). It was expected that data from these constructs would help anchor other elements of structure. Additionally, four of the sites chosen are located in helices that were poorly constrained in the previous analysis: Ec1 is located in P1; Ec95 and Ec101 are located in P8; and Ec316 is located in the loop of P18. All of the attachment sites are in highly conserved structural elements and thus were expected to provide information on the functional core of the ribozyme.

Circularly permuted RNase P RNAs were constructed as described previously (Harris et al., 1994). Briefly, circularly permuted DNA templates for in vitro transcription were generated by PCR amplification from tandem RNase P RNA genes. cpRNAs are expected to form the native structure, but contain a nick. Discontinuities in the ribose-phosphate backbone generally do not appear to alter the catalytic activity of RNase P RNA significantly (Waugh & Pace, 1993; Harris et al., 1994; Pan, 1995), indicating that the structure is maintained by secondary and tertiary interactions. Nevertheless, it was important to establish that the cpRNAs studied here reflect the native RNA structure accurately. This is indicated by their participation in the RNase P reaction. As shown in Table 1, the kinetic parameters k_{cat} and K_m for the cpRNAs used in this study are approximately native at elevated ionic strength. Most of the cpRNase P RNAs (Ec68, Ec95, Ec101, Ec244, Ec316) displayed 2–3-fold higher K_m values than the native RNA at 1 M monovalent salt, but exhibited near-native kinetic parameters at a higher salt concentration (Table 1 and data not shown). Because the rate of the RNase P RNA reaction in vitro is limited by release of product (Reich et al., 1988; Tallsjö & Kirsebom, 1993), increases in K_m also result in elevated k_{cat} values. The reduced affinity for substrate (increase in K_m) exhibited by some of the cpRNase P RNAs likely reflects an increased flexibility in the RNase P RNA chain due to interruption of the phosphodiester backbone. The high ionic strength suppresses the effect of the nick, presumably by screening repulsive forces that work to distort the cpRNA from its native structure.

TABLE 1. Catalytic activity of cpRNase P RNAs and analysis of crosslinked species.

Crosslinked species	Efficiency[a]	Activity k_{cat} (min^{-1})	Activity K_m (nM)	Crosslinked nucleotides	Constraint[b]
Native		0.199 ± 0.096	55 ± 14		
3′-ethNative.1	1.3	+		circle	
3′-ethNative.2	1.2	+		112,114,118	*A*
Ec68[c]		0.03 ± 0.011	189 ± 30		
5′-apa68.1	1.06[d]	+		10, 11	*B*
5′-apa68.2	0.5	+		359, 360	
5′-apa68.3	12.5	+		350–353	
5′-apa68.4	0.8	+/−		246, 247, 252, 253	
5′-apa68.t1	1.2	+/−		n/d	
3′-eth68.1	10.2[d]	+		343–351, 359, 360	
3′-eth68.2	4.3	+/−		328, 332, 333	
3′-eth68.3	2.5	+/−		304, 300, 299	
Ec95		0.512 ± 0.057	115 ± 1.5		
5′-apa95.1	1.0	+/−		circle	
5′-apa95.2	1.0	+		315,316	*C*
Ec101		0.366 ± 0.029	167 ± 12		
5′-apa101.1	3.1[d]	+		68, 69	*D*
5′-apa101.2	0.6	+		356, 357	*D*
5′-apa101.3[e]	1.2	+/−		233	
Ec244		0.186 ± 0.07	163 ± 33		
5′-apa244.1	0.7	+		circle	
5′-apa244.2	5.6	+		85–89	*E*
5.apa244.3	1.2	+		77–79	*E*
5′-apa244.4	>0.5	+		275, 276	*E*
Ec250		0.427 ± 0.069	73 ± 30		
5′-apa250.1	2.3	+		circle	
5′-apa250.2	1.6	+		51	*F*
5′-apa250.3	1.7	+		28, 29	*F*
5′-apa250.t1	1.5	+		tRNA −5 to +1	
5′-apa250.t2	1.6	+		n/d	
Ec316		0.348 ± 0.088	115 ± 41		
5′-apa	2.5	+		circle	

[a] Efficiency indicates percent conversion to crosslinked species.
[b] See Figure 6.
[c] Requires 100 mM Mg.
[d] Circular forms likely contribute to the efficiency of these crosslinked species.
[e] Not present when pre-tRNA binds.

One cpRNase P RNA, Ec68, required elevated concentrations of divalent metal ions for optimal in vitro activity. Even under optimal conditions, Ec68 still displayed a 6–10-fold lower k_{cat} than the native ribozyme (Table 1). Nucleotide 68 is located in helix P4, which is conserved in both sequence and structure, and contains phosphate oxygens flanking G68 that are important for RNase P RNA-mediated catalysis (Harris & Pace, 1995). Thus, it seems likely that the altered catalytic properties of Ec68 are due to local disruption of catalytically important structure rather than global misfolding. Consistent with this notion is the near-native K_m for this construct (Table 1) and the ability of Ec68 to form intermolecular crosslinks to photoagent-modified tRNA with the same efficiency as native RNase P RNA (data not shown). Nonetheless, we exercised care in interpreting crosslinking results obtained with this construct (see below). The crosslinking studies outlined below were performed under the optimal catalytic conditions for each cpRNA.

For crosslinking, an azidophenacyl (APA) group was attached to either the 5′ or 3′ end of individual cpRNAs. For 5′-modification, the APA group was attached to cpRNAs containing a 5′-phosphorothioate incorporated during transcription (Burgin & Pace, 1990). Inclusion of guanosine monophosphorothioate in transcription reactions results in its incorporation only at the 5′ end, because nucleoside monophosphates can initiate transcription, but are unable to be utilized for elongation by T7 RNA polymerase. The phosphorothioate sulfur provides a unique site in the RNA for the attachment of the azidophenacyl group. For 3′-modification, the photoagent was attached following oxidation of the 3′ end of the cpRNase P RNA and

reductive alkylation with ethylene diamine and attachment of a primary amine-specific photoagent (Oh & Pace, 1994). In either configuration, irradiation with 302-nm light converts the azido group to a highly reactive nitrene, which is able to insert into a variety of covalent bonds (Schuster & Platz, 1992).

Intramolecular crosslinking of 5′- or 3′-APA cpRNAs results in the formation of lariats, which can be separated from noncrosslinked RNA by PAGE. In order to characterize the crosslinking reactions, a number of control experiments were performed with each of the individual photoagent-modified cpRNAs. An example of these reactions for 5′-APA Ec244 RNA is presented in Figure 2A. As in the previous analysis, crosslinking of APA-modified cpRNase P RNAs was rapid, occurring with a $t_{1/2}$ of less than 5 min, and crosslinking occurred exclusively via the azidophenacyl moiety, because unconjugated RNA did not form

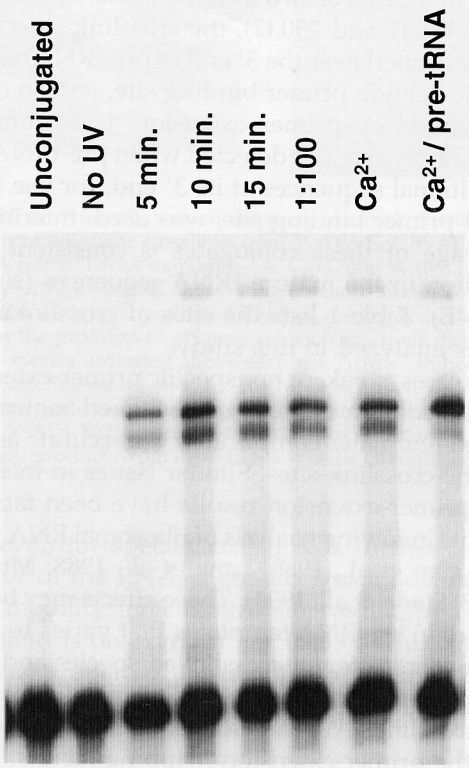

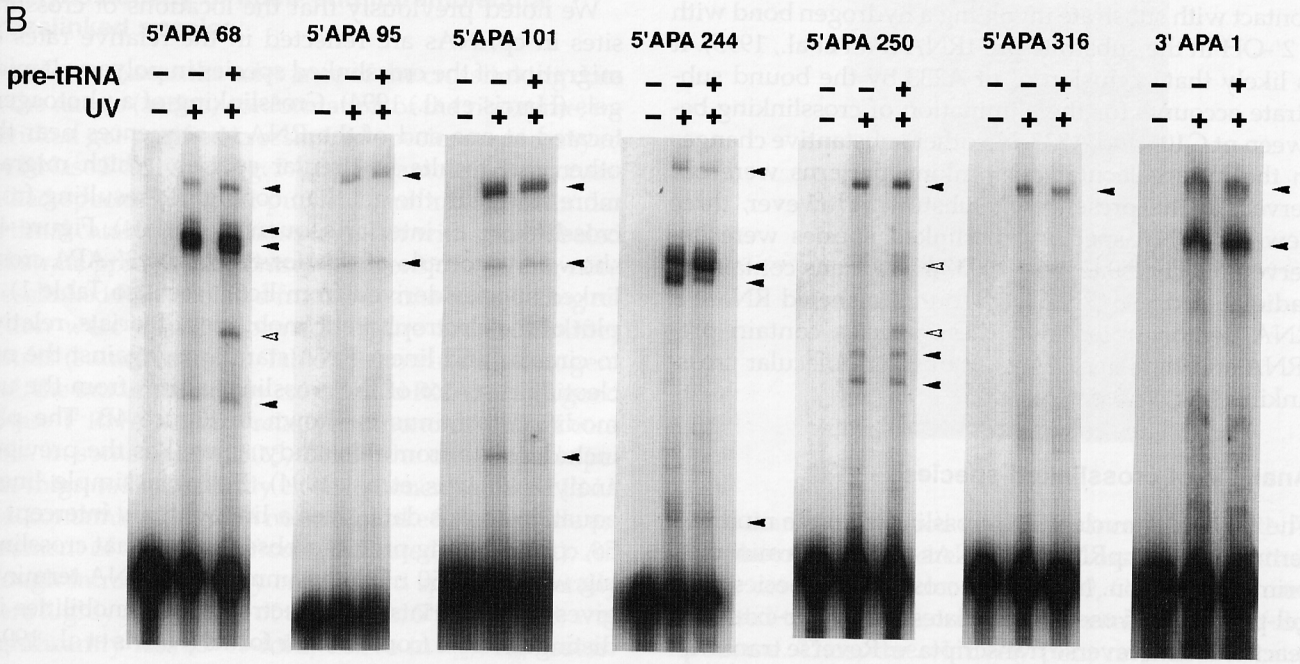

FIGURE 2. Identification of crosslinked species. **A:** Analysis of intramolecular crosslinking of 5′-azidophenacyl Ec244 RNA. Radiolabeled 5′-APA Ec332 cpRNase P RNA was crosslinked under in vitro RNase P RNA reaction conditions: 40 mM Tris-HCl, pH 8.0; 1 M ammonium acetate; 20 mM divalent metal ion as indicated; and 0.1% SDS. Crosslinked species and uncrosslinked RNA were resolved on denaturing acrylamide gels. The lane marked No UV was not exposed to 302-nm light; lanes marked 5 min, 10 min, and 15 min were irradiated for those lengths of time. The concentration of 5′-APA Ec332 RNA was 2 nM, except for the lane marked 1:100, which contained 0.02 nM RNA. The lane marked Ca^{2+} had Ca^{2+} replacing Mg^{2+} as the divalent ion. The lane marked Ca^{2+}/pre-tRNA contained nonradiolabeled pre-tRNA at 200 nM. The time of irradiation of the Unconjugated sample was 15 min and it contains Ec244 RNA, which was not modified with the APA photoagent. **B:** Radiolabeled 5′-APA cpRNase P RNAs at 2 nM were irradiated with 302-nm light for 15 min in either the presence (+) or absence (−) of 100 nM pre-tRNA. The reaction conditions are those described in Materials and Methods, except that $CaCl_2$ was substituted for $MgCl_2$ (Smith et al., 1992). The presence of $CaCl_2$ slows the catalytic rate without affecting pre-tRNA binding. The amount of pre-tRNA cleavage during the crosslinking reaction was less that 5%. Triangles to the right of each pair of lanes indicate the major crosslinked species. Open triangles indicate the position of pre-tRNA-specific crosslinked species.

crosslinks (Fig. 2A; data not shown). The formation of intramolecular crosslinks was tested by assessing the sensitivity of the crosslinking reaction to dilution (e.g., Fig. 2A, lane 1:100). The conversion of the analyzed RNAs containing the photoagent into crosslinked species was efficient, between 0.5% and 12% (Table 1). Figure 2B shows the crosslinking results obtained with all six 5′-APA cpRNase P RNAs and 3′-APA native RNase P RNA, alone and in the presence of substrate pre-tRNA. Some low-efficiency crosslinks that were not reproducible between experiments were detected occasionally. Only crosslinked species that were formed consistently were chosen for detailed analysis. These individual crosslinked species are designated numerically beginning with the species migrating most slowly in the gel (for example, crosslinked species detected using Ec68 are denoted 68.1, 68.2, 68.3, and 68.4).

The presence of substrate resulted in only small changes in the pattern of some crosslinked species (Fig. 2B). For this analysis, Ca^{2+} was substituted for Mg^{2+} to suppress cleavage and allow crosslinking to pre-tRNA. Substitution with Ca^{2+} had no detectable effect on the intramolecular crosslinks detected in the presence of Mg^{2+} (Fig. 2A and data not shown). A 5–7-fold decrease in the efficiency of the 244.2 crosslinked species was observed when the crosslinking reaction was performed with substrate present. One crosslinked species (101.3) was observed with 5′-APA Ec101 alone, but was not generated when the crosslinking reaction was performed in the presence of substrate. Primer-extension mapping of 101.3 demonstrated that the photoagent was crosslinked to nt A233 (see below; Fig. 3A). A233 is protected from chemical modification in the presence of substrate (LaGrandeur et al., 1994) and the homologous nucleotide in *Bacillus subtilis* RNase P RNA has been shown to form a direct contact with substrate involving a hydrogen bond with a 2′-OH in the substrate pre-tRNA (Pan et al., 1995). It is likely that occlusion of nt A233 by the bound substrate accounts for the elimination of crosslinking between nt G101 and A233. No other substantive changes in the intramolecular crosslinking patterns were observed in the presence of substrate. However, three new pre-tRNA-specific crosslinked species were observed (68.t1, 250.t2, and 250.t3). Reactions containing radiolabeled pre-tRNA and nonradiolabeled RNase P RNA demonstrated that these species contain pre-tRNA and thus are the result of intermolecular crosslinking (Fig. 6; see below).

Analysis of crosslinked species

The particular nucleotides crosslinked to the modified termini of the cpRNase P RNAs were determined by primer extension. Individual crosslinked species were gel-purified and used as templates for primer-extension reactions with reverse transcriptase. Reverse transcriptase terminates one nucleotide 3′ to crosslink sites in the RNA template (Burgin & Pace, 1990 and references therein). Examples of this analysis for the crosslinked species derived from Ec1, Ec101, and Ec250 are shown in Figure 3A. Intermolecular crosslinks were mapped by primer extension using pre-tRNA-specific oligonucleotide primers. An example of the primer-extension results for the 250.t1 conjugate is shown in Figure 3B. Comparison of extension products from crosslinked RNA with reaction products from noncrosslinked RNA and sequencing reactions identifies the individual crosslinked nucleotides. For two intermolecular crosslinked conjugates (68.t1 and 250.t2), the crosslink sites were apparently located near the 3′ end of pre-tRNA, within the oligonucleotide primer binding site, and so could not be mapped by primer extension. Unfortunately, these crosslinks were not detected when pre-tRNA carrying additional sequences at its 3′ end, for use as an additional primer binding site, was used. Intermolecular cleavage of these conjugates is consistent with their location in the mature tRNA sequences (see below; Fig. 4B). Table 1 lists the sites of crosslinking in the species analyzed in this study.

In some cases, weak, or nonspecific primer-extension stops observed both in the noncrosslinked control and crosslinked templates complicated the accurate assessment of the crosslink sites. Similar issues in interpretation of primer-extension results have been faced in experiments involving analysis of ribosomal RNA structure (Denman et al., 1988; Lane et al., 1988; Mitchell et al., 1993; Stade et al., 1994). These effects may be due to structure in the RNA templates that varies to some extent between different crosslinked species and even between preparations of RNA or chemical decomposition of crosslinks. We therefore sought results to corroborate the primer-extension mapping results.

We noted previously that the locations of crosslink sites in cpRNAs are reflected in the relative rates of migration of the crosslinked species in polyacrylamide gels (Harris et al., 1994). Crosslinking of a photoagent located at one end of the RNA to sequences near the other end results in circular species, which migrate more slowly in the gel than conjugates resulting from crosslinking to interior sequences (lariats). Figure 4A shows an example of this for the major 3′-APA crosslinked species derived from Ec68 (see also Table 1). A plot of the electrophoretic mobilities of lariats, relative to circular and linear RNA standards, against the nucleotide distance of the crosslinked sites from the unmodified terminus is shown in Figure 4B. The plot includes data from this study, as well as the previous analysis (Harris et al., 1994). Fitting a simple linear equation to this data gives a line with a y intercept of 56, corroborating previous observations that crosslinking within 50–60 nt of the unmodified RNA terminus gives rise to lariats with electrophoretic mobilities indistinguishable from circular forms (Harris et al., 1994).

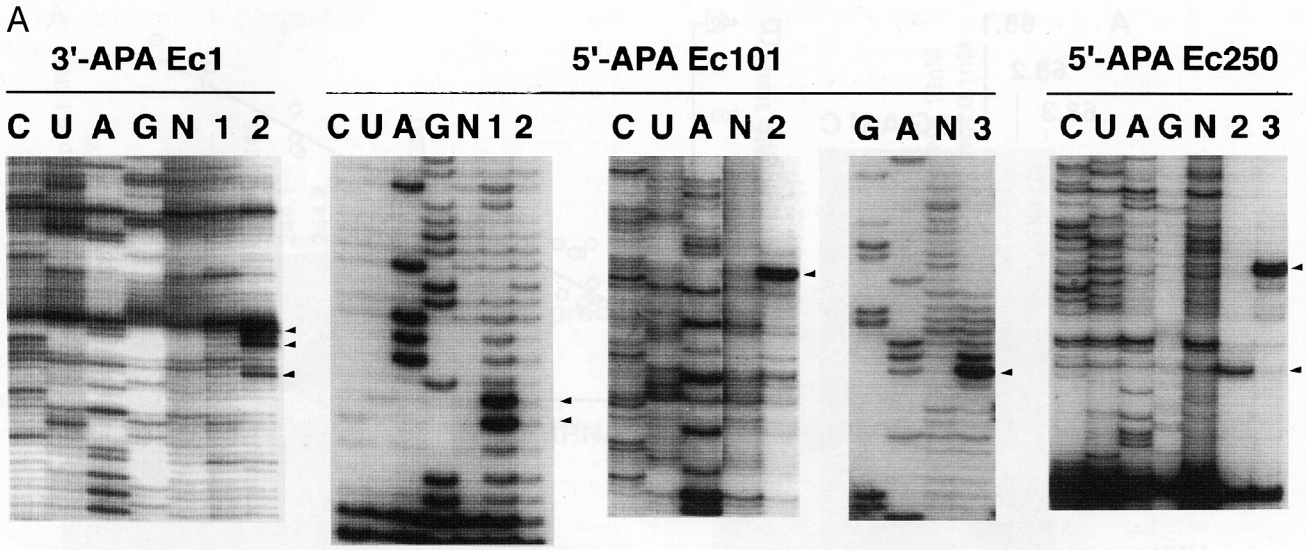

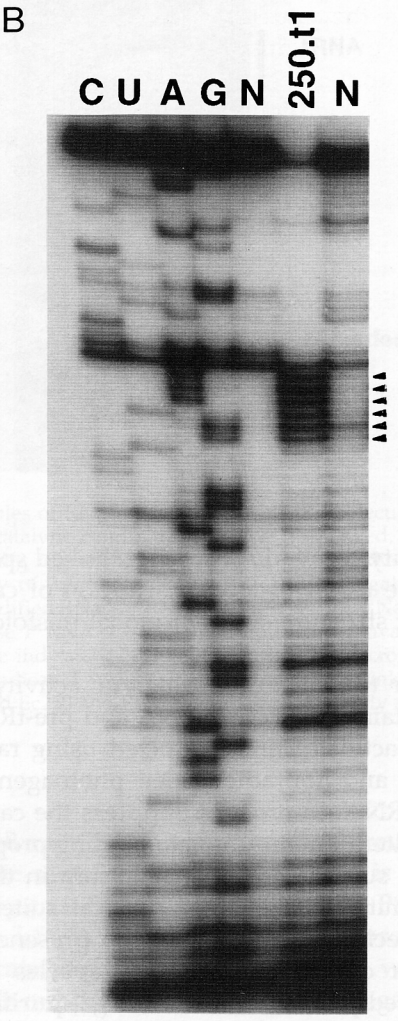

FIGURE 3. Primer-extension mapping of crosslink sites. **A:** Analysis of intramolecular crosslinks from 3′-APA Ec1, 5′-APA Ec101, and 5′-APA Ec250. Lanes marked G, A, C, U, and N denote lanes containing G, A, C, and U sequencing reactions and a control primer extension with noncrosslinked RNA, respectively. Numbered lanes contain the products of primer-extension reactions using the crosslinked species indicated above each gel. Arrows indicate the positions of terminations specific to the crosslinked RNA templates. **B:** Primer extension mapping of intermolecular crosslinking between 5′-APA Ec250 and pre-tRNA. Lanes are marked as in A and represent products from a pre-tRNA specific oligonucleotide primer.

However, for species crosslinked further toward the interior of the RNA, a good correspondence between lariat mobility and crosslink sites as mapped by primer extension is observed ($r^2 = 0.939$). Thus, the electrophoretic properties of the different crosslinked species offer confirmation of the primer-extension results.

Catalytic activity of inter- and intramolecular crosslinked species

In order to assess the relevance of the crosslinking data to the native (active) conformation of the ribozyme, individual gel-purified crosslinked species were assayed for RNase P activity (Fig. 5A,B). Intramolecularly crosslinked species were gel-purified and incubated under optimal catalytic conditions together with radiolabeled substrate pre-tRNA. Control reactions containing noncrosslinked RNA isolated from the same crosslinking reaction were also performed. Figure 5A exemplifies results (summarized in Table 1) showing that, in general, the intramolecularly crosslinked RNAs retain good RNase P RNA activity relative to noncrosslinked controls. In some cases (250.3, 244.3), the crosslinked species migrated sufficiently close to noncrosslinked RNA that contamination with noncrosslinked RNA made assessment of activity difficult (indicated in Table 1). Although intramolecularly crosslinked species generally were highly active, one of the RNAs, 5′-APA Ec68, was significantly less (5–10-fold) active in k_{cat}/K_m assessments than control reactions using noncrosslinked RNA. The photoagent attached at G68 crosslinked to other highly conserved nucleotides (G350, C247), which are expected to comprise, in part, the catalytic core of the ribozyme. Thus, the relatively poor retention of cata-

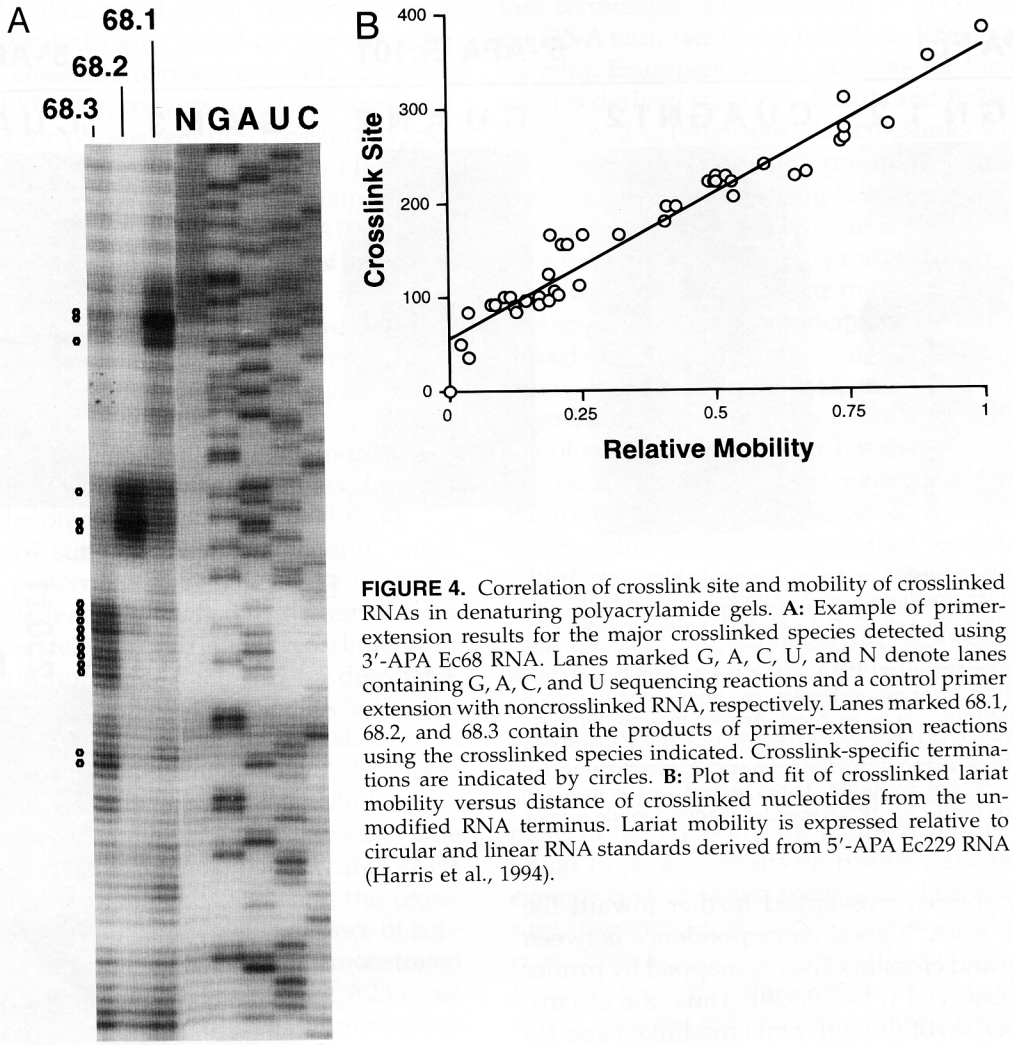

FIGURE 4. Correlation of crosslink site and mobility of crosslinked RNAs in denaturing polyacrylamide gels. **A:** Example of primer-extension results for the major crosslinked species detected using 3′-APA Ec68 RNA. Lanes marked G, A, C, U, and N denote lanes containing G, A, C, and U sequencing reactions and a control primer extension with noncrosslinked RNA, respectively. Lanes marked 68.1, 68.2, and 68.3 contain the products of primer-extension reactions using the crosslinked species indicated. Crosslink-specific terminations are indicated by circles. **B:** Plot and fit of crosslinked lariat mobility versus distance of crosslinked nucleotides from the unmodified RNA terminus. Lariat mobility is expressed relative to circular and linear RNA standards derived from 5′-APA Ec229 RNA (Harris et al., 1994).

lytic activity by 5′-APA Ec68 crosslinked species probably is the result of local disruption of catalytically important structure, and not global misfolding of the RNA.

In order to analyze the catalytic activity of conjugates containing RNase P RNA and pre-tRNA, crosslinking reactions were conducted using radiolabeled pre-tRNA and nonradiolabeled photoagent-modified RNase P RNA. In order to suppress the catalytic rate without alteration of substrate-binding properties, calcium was substituted for magnesium in the reaction buffer (Smith et al., 1992). Identical suites of crosslinked species are formed in the presence of magnesium or calcium. Crosslinked species containing radiolabeled pre-tRNA then were gel-purified and incubated under standard in vitro RNase P RNA reaction conditions containing magnesium, at dilute concentrations of RNA (0.1 nM) and for short incubation times (5 min) to minimize cleavage of pre-tRNA in trans. Under these conditions, almost no cleavage of pre-tRNA occurs in control intermolecular RNase P RNA cleavage reactions (Fig. 5B). Intramolecular cleavage of crosslinked pre-tRNA within the conjugate should release a specific fragment, depending on the location of the crosslink. For example, conjugates formed by crosslinking between the photoagent and nucleotides in the 5′ leader sequences should release the mature tRNA fragment. Species generated by crosslinking within the mature domain should release the 5′ leader fragment. Figure 5B shows the results from intermolecular crosslinks derived from Ec250 and Ec68, as well as two intermolecular crosslinks, derived from Ec292 and Ec332, which were described previously (Harris et al., 1994).

Although all of the gel-purified intermolecular crosslinked conjugates are contaminated (1–5%) by noncrosslinked or spontaneously decoupled (Burgin & Pace, 1990) pre-tRNA, each releases the predicted fragment based on the location of the intermolecular crosslink, after incubation under RNase P RNA assay conditions. 332.t1 and 250.t1 were generated by crosslinking within the 5′ leader sequence and, upon cleavage, release the mature tRNA fragment. In contrast, 292.t1, 250.t2, and 68.t1 result from crosslinking within the mature do-

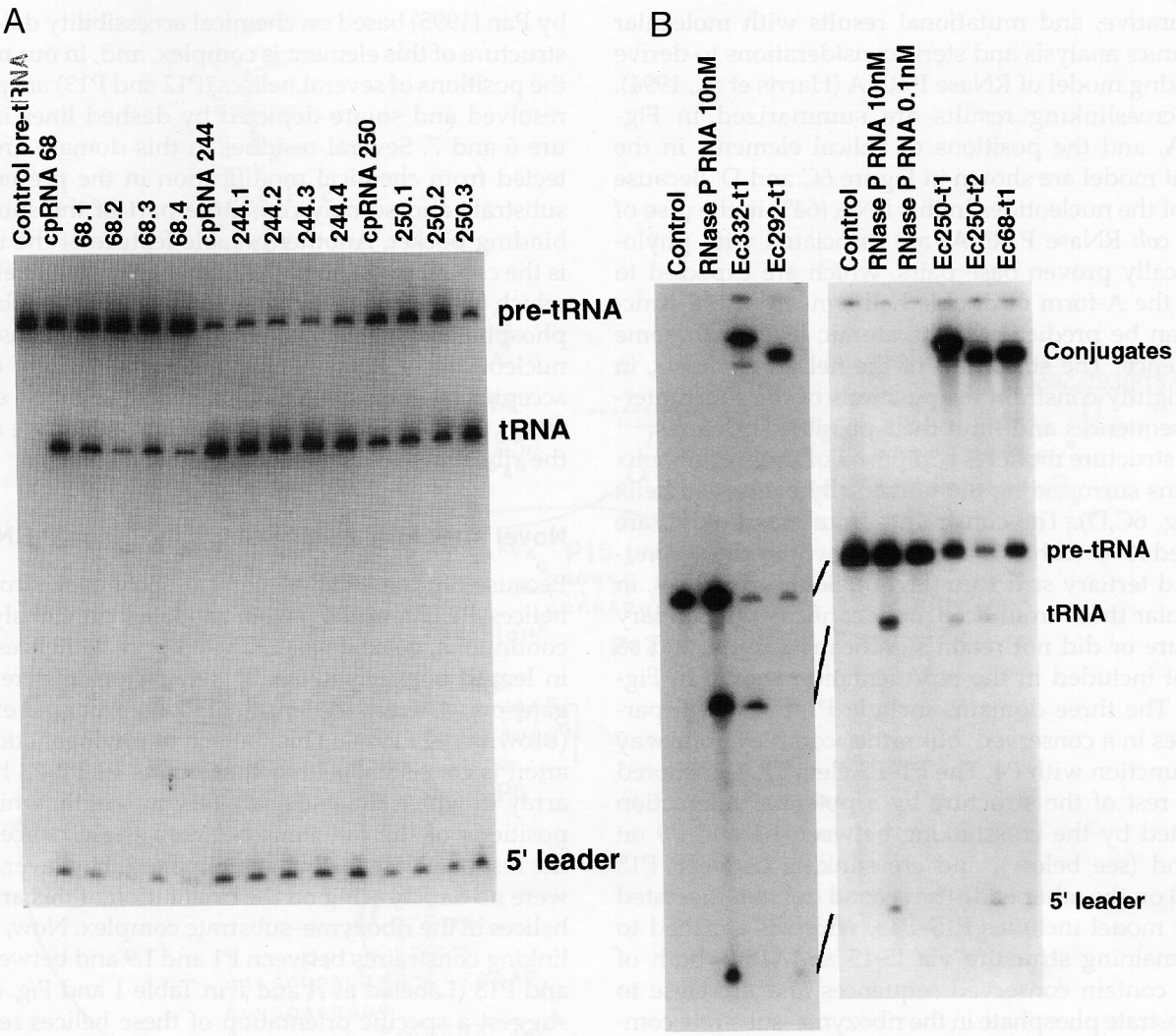

FIGURE 5. Analysis of the catalytic activity of crosslinked RNAs. **A:** Examples of RNase P assays using intermolecular crosslinked species. Radiolabeled pre-tRNA was incubated under optimal catalytic conditions with the crosslinked, or control noncrosslinked species as indicated. Positions of bands corresponding to pre-tRNA, mature tRNA, and the 5′ leader sequence are indicated at right. **B:** Analysis of the catalytic activity of intermolecular crosslinked conjugates. Gel-purified intermolecular crosslinked conjugates containing photoagent-modified RNase P RNA and radiolabeled RNase P RNA were incubated under optimal catalytic conditions for native RNase P RNA. Control intermolecular cleavage reactions containing native RNase P RNA and noncrosslinked pre-tRNA are indicated. Positions of radiolabeled crosslinked conjugates, pre-tRNA, mature tRNA, and the 5′ leader fragment are indicated at right. Intermolecular crosslinked conjugates derived from 5′-APA Ec292 and Ec332 from Harris et al. (1994), and Ec250 and Ec68 from the present study are shown.

main and release the 5′ leader fragment. Taken together, the catalytic activities of inter- and intramolecularly crosslinked species strongly support the interpretation that the crosslinking results reflect the structure of the native ribozyme.

DISCUSSION

These experiments extend significantly the library of structural constraints that bear on the structure of the *E. coli* RNase P ribozyme–substrate complex. The results support three new structural features that models of the RNase P ribozyme–substrate complex must accommodate. The first feature involves an interaction between L18 and P8 that was identified previously by phylogenetic sequence comparisons and is now corroborated by crosslinking between G95, in P8, and nucleotides in L18. A second feature is the proximity of P8 to the catalytic core of the ribozyme, which was suggested in our previous model, but now gains direct experimental support. The third new structural feature is the orientation of the P1-P2-P3 element, which is now anchored at both ends by crosslinks between P1 and P9, and between P15 and P3, consistent with recent crosslinking results using *B. subtilis* RNase P RNA (J.-L. Chen, M.E. Harris, & N.R. Pace, unpubl.). Previously, we have described the use of crosslinking,

comparative, and mutational results with molecular mechanics analysis and steric considerations to derive a working model of RNase P RNA (Harris et al., 1994). New crosslinking results are summarized in Figure 6A, and the positions of helical elements in the current model are shown in Figure 6C and D. Because most of the nucleotides in this RNA (64% in the case of the *E. coli* RNase P RNA) are associated with phylogenetically proven base pairs, which are expected to adopt the A-form of double helix, much of the structure can be predicted at the atomic level with some confidence. The structures of the helical elements, in turn, tightly constrain the positions of the short interhelix sequences and limit their possible structures.

The structure model is composed of three multihelix domains surrounding the universally conserved helix P4 (Fig. 6C,D). The constraints from crosslinking are denoted *A–G* (Table 1) and are shown on the secondary and tertiary structure (Fig. 6). Some crosslinks, in particular those from Ec68, only confirmed secondary structure or did not retain significant activity, and so are not included in the representation shown in Figure 6. The three domains include P1–P3, which participates in a conserved, but rather complex, four-way helix junction with P4. The P1–P3 element is anchored to the rest of the structure by a potential interaction indicated by the crosslinking between P1 and P9 on one end (see below), and crosslinking between P15 and P3 on the other end. The second domain indicated by the model includes P15–P18, which is attached to the remaining structure via J5-15 and J18-2, both of which contain conserved sequences and are close to the substrate phosphate in the ribozyme–substrate complex (Burgin & Pace, 1990; Harris et al., 1994). The CCA binding site is located in this domain in the P15–P16 internal bulge. The distal ends of P15–P18 are variable phylogenetically. In *E. coli* RNase P RNA, one end of the P15–P18 element participates in the long-range P6 pairing interaction. The other end is anchored via a GNRA tetraloop interaction between P18 and P8 (Brown et al., 1996; see also Fig. 7B). The third domain includes P7–P14 and corresponds to Domain I proposed by Pan (1995) based on chemical accessibility data. The structure of this element is complex, and, in our model, the positions of several helices (P12 and P13) are poorly resolved and so are depicted by dashed lines in Figure 6 and 7. Several residues in this domain are protected from chemical modification in the presence of substrate and so may constitute part of the substrate binding pocket. Another notable feature of the model is the central position of the highly conserved helix P4, which is located immediately adjacent to the substrate phosphate (Figs. 6C, 7A). This draws many conserved nucleotides in RNase P RNA into the vicinity of the acceptor stem of the tRNA, consistent with the expectation that conserved sequences form the active site of the ribozyme.

Novel structural relationships in RNase P RNA

Because of their proximity in the secondary structure, helices P1, P2, and P3 were modeled previously as a continuous, coaxial stack. The P1 and P3 helices vary in length between RNase P RNAs from different organisms, whereas the length of P2 is conserved exactly (Brown et al., 1994). This pattern of phylogenetic variation is consistent with a continuous P1-P2-P3 helical array in which the ends can vary in length, while the positions of the junctions between these helices and the rest of RNase P RNA remain fixed. However, there were no data bearing on the orientation of this array of helices in the ribozyme–substrate complex. Now, crosslinking constraints between P1 and L9 and between P3 and P15 (Labeled as *A* and *F* in Table 1 and Fig. 6C,D) suggest a specific orientation of these helices relative to the rest of the RNA (Fig. 7A). The phylogenetic volatility of the lengths of P1 and P9 suggest that they are both oriented toward the exterior of the structure, yet there is some evidence to suggest that they participate in a specific interaction (see below). The sequence-length of P3 also varies dramatically, however, P15 is largely conserved. Thus, it is somewhat surprising to observe crosslinking between these two structural elements. Nonetheless, crosslinking between homolo-

FIGURE 6. Overview of crosslinking results and structural interpretation. **A:** Overview of structural information from this study. Structural constraints from this study are indicated in blue by curved lines connecting crosslink attachment sites (stars) and crosslink sites (brackets). Letters indicating crosslinking constraints correspond to the "Constraint" column of Table 1. Lines connecting the paired halves of P4 and P6 are omitted for clarity (see Fig. 1). **B:** Secondary structure diagram of tRNA indicating known intermolecular interactions. Nucleotide positions that can be deleted without significantly altering recognition by RNase P RNA are shown as open circles. The RNase P cleavage site is indicated by an arrow. Nucleotide positions where base-identity is important are indicated by the appropriate letter. The sites of two interactions between the substrate and the ribozyme are indicated by green dotted lines and the corresponding nucleotide position in RNase P RNA is indicated (Kirsebom & Svärd, 1994; Pan et al., 1995). **C,D:** Structure model generated by manual computer modeling with refinement. Part C shows the substrate binding face of the structure and D is rotated 180° about the *y* axis relative to the structure depicted in C. Positions of helices in RNase P RNA are indicated by cylinders labeled according to the secondary structure diagram; only the proximal portion of helix P3 is shown. The backbone of tRNA is indicated in red by a ribbon; only the acceptor and TyC stems are shown for clarity. The position of the substrate phosphate is indicated by a red sphere. Constraints are shown in blue and labeled with letters corresponding to the secondary structure diagram in A and the "Constraint" column in Table 1. Helices P12–P15 are indicated by dotted lines because the available information is not sufficient to suggest useful conformations of this portion of the molecule.

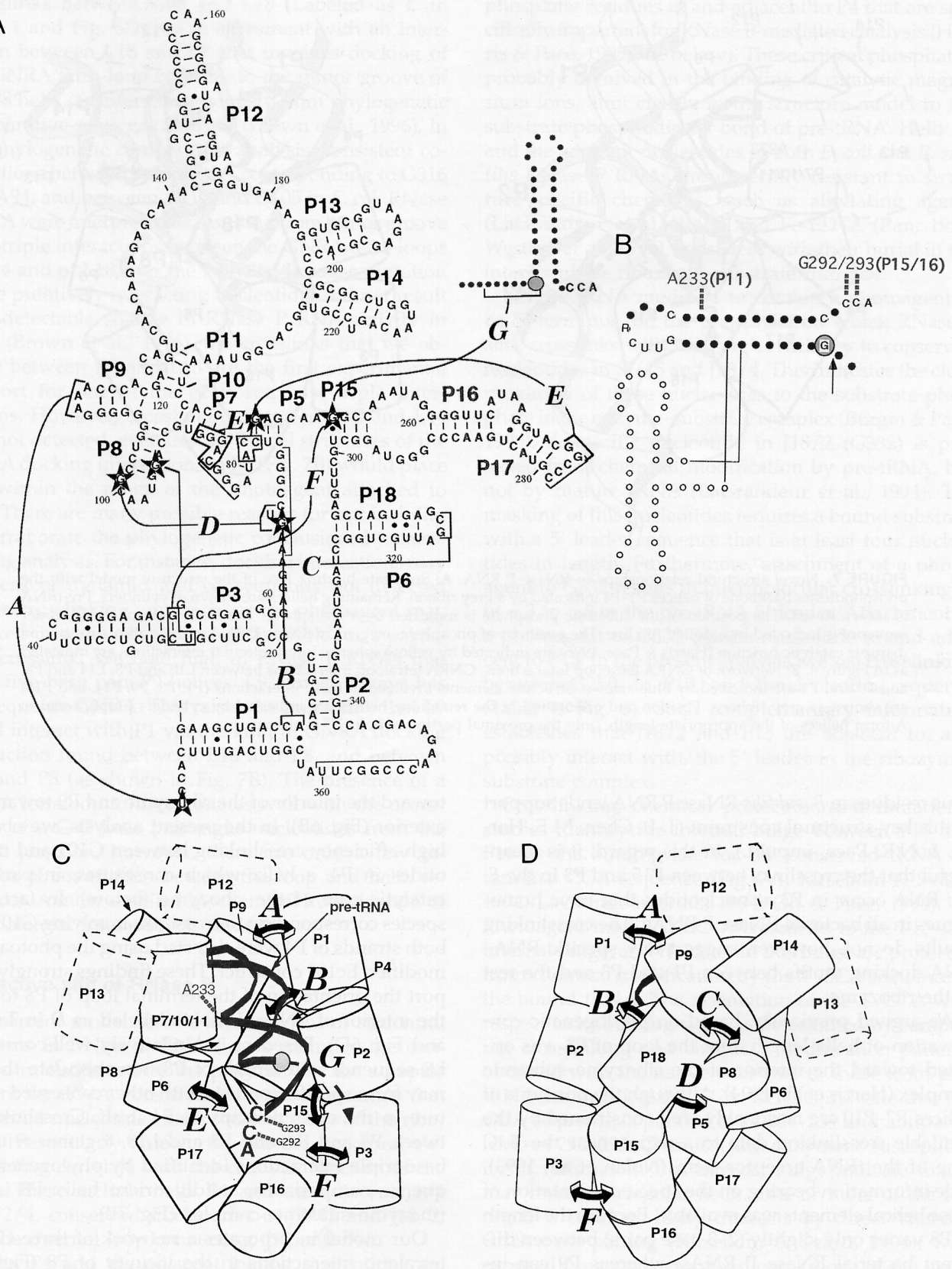

FIGURE 6. (*Legend on facing page.*)

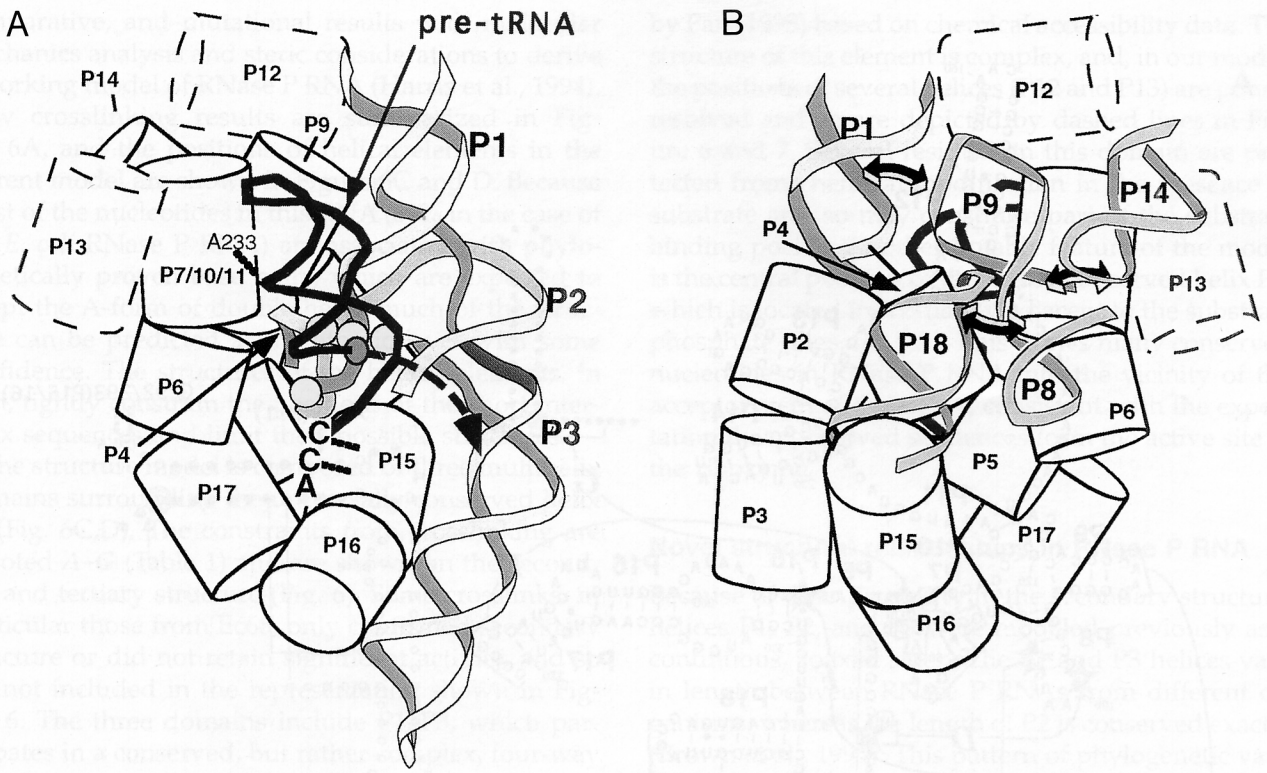

FIGURE 7. Novel structural relationships in RNase P RNA. **A:** Substrate binding face of the structure model with the phosphodiester backbone of helices P1–P4 indicated by a grey ribbon. Remaining helices are shown as cylinders. Pre-tRNA is shown in red. The position of the substrate phosphate is indicated by a red sphere. The likely path of the 5′ leader sequence is indicated by a dotted red line. The positions of phosphate oxygens in RNase P RNA where sulfur substitution disrupts catalytic function (Harris & Pace, 1995) are indicated by yellow spheres. Intermolecular interactions are indicated as in Figure 6. **B:** Network of GNRA tetraloop interactions. GNRA tetraloop interactions between L18 and P8, L14 and P8, and P9 and P1 are indicated by blue arrows. Structure elements involved in these interactions (P1, P8, P9, P14, and P18) are shown as grey ribbons. Position and orientation of the remaining helices are indicated by cylinders proportional to A-form helices of the appropriate length; only the proximal portion of helix P3 is shown.

gous residues in *B. subtilis* RNase P RNA lends support to this key structural constraint (J.-L. Chen, M.E. Harris, & N.R. Pace, unpubl.). In this regard, it is meaningful that the crosslinks between P15 and P3 in the *E. coli* RNA occur in P3 at nucleotides that have homologues in all bacterial RNase P RNAs. The crosslinking results do not, however, suggest any specific RNA–RNA docking motifs between P1 and P3 and the rest of the ribozyme.

We argued previously, based on phylogenetic conservation of helix-length, that the loop of P8 was oriented toward the interior of the ribozyme–substrate complex (Harris et al., 1994). Although the positions of helices P7–P10 are reasonably well-constrained by the available crosslinking data to a region near the TψC loop of the tRNA acceptor stem (Nolan et al., 1993), little information bearing on the specific orientation of these helical elements was available. Because the length of P8 varies only slightly (2–3 base pairs) between different bacterial RNase P RNAs, whereas P9 can increase dramatically in length (to more than 20 base pairs) (Brown et al., 1994), phylogenetic data are consistent with an arrangement whereby P8 is oriented toward the interior of the ribozyme and P9 toward the exterior (Fig. 6B). In the present analysis, we observe high-efficiency crosslinking between G101 and nucleotides in P4, a helix which constitutes, in part, the catalytic core of the ribozyme (below). In fact, two species corresponding to crosslinks involving G101 and both strands of P4 were detected using the photoagent-modified Ec101 construct. These findings strongly support the orientation of the terminal loop of P8 toward the interior of RNase P RNA (labeled as ***D*** in Table 1 and Fig. 6D). Based on the relatively well-conserved L8 sequence and length of P8, we speculate that L8 may form specific contacts with other conserved structure in the core, perhaps in P4 itself. Crosslinks between P8 and P4, and P8 and L18, together with the base-triple interactions identified by phylogenetic sequence comparisons, solidly orient helix P8 in the ribozyme–substrate complex (Fig. 7B).

Our model incorporates a network of three GNRA tetraloop interactions in the vicinity of P8 (Fig. 7B). This kind of RNA–RNA interaction was first postulated for Group I and Group II introns (Michel & Westhof, 1990; Costa & Michel, 1995), and so appears

to be a common architectural motif in large RNAs. Crosslinks between G95 and L18 (Labeled as *C* in Table 1 and Fig. 6D) are in agreement with an interaction between L18 and P8 that involves docking of the GNRA tetra-loop of P18 into the minor groove of the P8 helix, as inferred previously from phylogenetic comparative sequence analysis (Brown et al., 1996). In the phylogenetic comparative analysis, consistent covariations between nucleotides corresponding to G316 and A94, and between A214 and G105 in *E. coli* RNase P RNA were interpreted as resulting from minor groove base-triple interactions between the GNRA tetra-loops of L14 and of L18, and the P8 helix. Because mutation of the putatively interacting nucleotides did not result in a detectable change in RNase P RNA activity in vitro (Brown et al., 1996), the crosslinks that we observe between P8 and L18 are the first experimental support for one of the proposed base-triple interactions. However, crosslinking between G95 and L14 was not detected, even though model structures of the GNRA docking interactions in P8 (Fig. 7B) would place L14 within the range of the photoagent attached to G95. There are many possible reasons for our inability to corroborate the phylogenetic conclusions by crosslinking analysis. For instance, docking interactions may be weak or dynamic, and consequently not detected by the crosslinking approach; or the photoagent may be fixed in some orientation unfavorable for a particular crosslink. We note that, in RNase P RNAs that have five base pair P9 helices, L9 almost always has the sequence GNRA. This raises the possibility that L9 could interact with P1 via the kind of GNRA docking interaction found between L18 and P8, and between L14 and P8 (as shown in Fig. 7B). The presence of a GNRA tetraloop in L9 correlates well with the occurrence of a G-C base pair eight nucleotides from the P1–P2 junction; however, there are only a few instances of covariation beween the loop and helix sequences. A more detailed biochemical investigation of this potential interaction is underway.

The active site of RNase P

Our current model for the arrangement of structural elements in RNase P RNA draws many of the conserved nucleotides into the proximity of the acceptor stem of the tRNA, consistent with the expectation that conserved nucleotides form the active site of the ribozyme. Particularly noteworthy are the structural elements that correlate with the catalytic function of the RNA. These include helix P4 and the adjacent J3/4 and J2/4, conserved nucleotides in J5/15 and J18/2, and the internal loop connecting P15 and P16.

Helix P4 and the adjacent joining nucleotides are seen to constitute the heart of the active site of RNase P. This structural element includes the highest concentration of conserved nucleotides in the RNA, and recent modification-interference results have identified phosphate residues in and adjacent to P4 that are specifically important for RNase P-mediated catalysis (Harris & Pace, 1995; see below). These critical phosphates, probably involved in the binding of catalytic magnesium ions, abut closely in the structure model to the substrate phosphodiester bond of pre-tRNA. Helix P4 and the adjacent nucleotides in both *E. coli* and *B. subtilis* RNase P RNAs are generally resistant to structure-specific chemicals, such as alkylating agents (LaGrandeur et al., 1994) and Fe-EDTA (Pan, 1995; Westhof et al., 1996), consistent with their burial in the interior of the ribozyme–substrate complex.

Mature tRNA modified to contain a photoagent at its 5′ terminus, on the phosphate on which RNase P acts, crosslinks with very high efficiency to conserved nucleotides in J5/15 and J18/4. This indicates the close proximity of these nucleotides to the substrate phosphate in the enzyme–substrate complex (Burgin & Pace, 1990). A specific nucleotide in J18/2 (G332) is protected from chemical modification by pre-tRNA, but not by mature tRNA (LaGrandeur et al., 1994). The masking of this nucleotides requires a bound substrate with a 5′ leader sequence that is at least four nucleotides in length. Furthermore, attachment of a photoagent to G332 results in intermolecular crosslinking to nt −3 to −6 in the pre-tRNA 5′ leader. Attachment of a photoagent to G332 detects nucleotide in and adjacent to P15. In the present analysis, we see crosslinking between G250, in P15, and the 5′ leader sequence (Table 1; Fig. 6). Such complementary information establishes that J18/2 and P15 are adjacent to, and possibly interact with, the 5′ leader in the ribozyme–substrate complex.

Crosslinking, chemical protection, and mutational studies identify the internal bulge between P15 and P16 as the binding site for the conserved tRNA 3′-terminal CCA sequence (Fig. 7A, Kirsebom & Svärd, 1994; LaGrandeur et al., 1994; Oh & Pace, 1994). 3′-Photoagent-modified tRNA crosslinks to the P15–P16 internal bulge, and residues in this bulge are protected from chemical modification by the 3′ CCA sequence of the bound tRNA. The orientation of the 3′ CCA with respect to its binding site was determined by comparing crosslinking and chemical modification patterns obtained with the native substrate to those from pre-tRNA mutants lacking CCA. Results indicate that the CCA sequence is parallel to nt 254–259 and antiparallel to nt 290–295. Chemical and enzymatic susceptibility of residues in this internal bulge indicate that it may form an irregular helix. One or more of the terminal C residues likely interacts by direct Watson-Crick base pairing (Kirsebom & Svärd, 1994), with exposed functional groups in one groove of the irregular helix formed by the P15 and P16 connecting internal bulge. NMR analysis of this internal loop isolated from the remaining structure failed to detect a unique

conformation of this region in the absence of bound CCA. Recently, a theoretical model of the P15–P16 internal bulge with CCA bound, based on the available phylogenetic, mutational, and chemical crosslinking data, was proposed (Easterwood & Harvey, 1997). Crosslinking constraints between G250, in P15, and nucleotides in P3, and between the pre-tRNA substrate phosphate and J5/15, together with primary and secondary structural constraints, were used to position the CCA binding-site model relative to the rest of the helical array (Fig. 6C). The structure formed by the 3′-CCA and its docking site in the ribozyme–substrate complex also is evidently somehow important in the reaction mechanism; mutants in the substrate CCA influence the rate of the chemical step of the RNase P reaction (B.-K. Oh & N.R. Pace, in prep.).

Conclusion

The current structural perspective on RNase P RNA summarized in Figures 6 and 7 is consistent with a large body of experimental information, but it will sharpen with additional data; each new high-efficiency crosslink is an anchoring constraint in the structure model. Currently, only about 5% of the nucleotides in the bacterial RNase P RNA have been tested for crosslinking. Yet, already the core helices in the ribozyme are oriented with good resolution (ca. 5 Å) with respect to one another and the substrate (Harris et al. 1994). Peripheral helices are less well-ordered, but nonetheless are placed fairly accurately. A considerable part (ca. nt 130–230) of the RNase P RNA remains poorly defined in the current model because insufficient structural information is available. The general approach of phylogenetic–comparative analysis coupled with site-specific crosslinking is an important avenue in the study of large RNAs. The perspective is that results, even though at less than atomic resolution, define structural elements for finer attention, and global architectural features important for function. Coupled with modeling based on crystallographic studies, comparative and crosslinking data provide credibly detailed structural hypotheses for experimental test.

MATERIALS AND METHODS

Preparation and analysis of circularly permuted RNAs

Circularly permuted RNase P RNAs were generated essentially as described in Harris et al. (1994). Briefly, template DNAs for in vitro transcription were synthesized by PCR from tandemly repeated RNase P RNA genes. The two primers define the endpoints of the PCR product and thus the 5′ and 3′ ends of the transcribed RNA. The upstream primer contained the core promoter for phage T7 RNA polymerase. PCR reactions contained 30 mM Tris-HCl, pH 8.3, 1 mM dNTPs, 50 mM potassium chloride, 1.5 mM magnesium chloride, 0.05% NP-40, 1–10 pg tandem RNase P RNA or tRNA genes, and 100 pmol of the forward and reverse primers. The following primers were used:

Ec68fwd-5′-TAATACGACTCACTATAGTCCGGGCTCCATAGGGC-3′;
Ec68rev-5′-TTTCCTCCCCTCCGCCCGTC-3′;
Ec95fwd-5′-TAATACGACTCACTATAGGTAACGCCTGGGGGGGAA-3′;
Ec95rev-5′-TGGCACCCTGCCCTATGGAG-3′;
Ec101fwd-5′-TAATACGACTCACTATAGCCTGGGGGGGAAACCCACGA-3′;
Ec101rev-5′-GTTACCTGGCACCCTGCCC-3′;
Ec244fwd-5′-TAATACGACTCACTATAGAGCAAGGCCAAATAGGGG-3′;
Ec244rev-5′-CGGGTGGAGTTTACCGAG-3′;
Ec316fwd-5′-TAATACGACTCACTATAGATTGCTGGCCTAGATGA-3′;
Ec316rev-5′-GCTACATGGCTCAAGCAG-3′.

Circularly permuted RNase P RNA genes were cloned in a specially constructed vector, pSBF, which contained *Bbs* I and *Fok* I restriction enzyme sites strategically positioned downstream from a *Sma* I site. Cloning of these PCR DNAs into the *Sma* I site allowed the use of the *Fok* I or *Bbs* I sites to generate templates for in vitro transcription that were linearized precisely at the insert-vector junction. pEc250 was a generous gift from Dr. Dan Frank. The RNAs used in this study were prepared by in vitro transcription using phage T7 RNA polymerase as described (Harris et al., 1994).

cpRNase P RNAs were assayed for enzymatic activity in 10-μL reactions containing 1 nM RNase P RNA, 1 M or 3 M ammonium acetate, 25 mM magnesium chloride, 40 mM Tris-HCl, pH 8.0, 0.1% SDS, and 10 nM to 1 μM substrate pre-tRNA. Reactions were incubated for a length of time that effected no more that 20–30% cleavage of substrate (typically 5–10 min). Separation of substrate and cleaved products was accomplished by electrophoresis though 8% polyacrylamide/8 M urea gels. Gels were dried and conversion of pre-tRNA to cleaved products was analyzed using a Molecular Dynamics Phosphorimaging system. The kinetic parameters k_{cat} and K_m were extracted by plotting 1/velocity versus velocity/[substrate] (Eadie/Hofstee).

Crosslinking

Crosslinking experiments were performed essentially as described previously (Burgin & Pace, 1990; Oh & Pace, 1994). Briefly, for 5′-modification, an azidophenacyl group was conjugated to the unique sulfur at the 5′-terminal phosphate of 5′-guanosine monophosphorothioate (GMPS) RNAs. 5′-GMPS RNAs were generated by in vitro transcription in the presence of GMPS. 3′-Modification was accomplished by oxidation of the cpRNase P RNA followed by alkylation with ethylene diamine and attachment of a primary amine-specific photoagent, *p*-azidobenzoate succinamide ester. For crosslinking, the conjugated RNA was incubated under in vitro RNase P assay conditions (described above) at 65 °C for 2 min, then 37 °C for 10 min, followed by exposure to 302-nm light at 25 °C. Analytical reactions contained 2–0.02 nM 5′-APA cpRNase P RNA and were irradiated for 0.5–30 min. Preparative reactions contained 400 nM 5′-APA cpRNase P

RNA and were irradiated for 30 min. Pre-tRNA was included in the reactions as described in the figure legends. Calcium chloride replaced magnesium chloride in reactions containing pre-tRNA in order to suppress cleavage of the substrate (Smith et al., 1992). Gel-purified crosslinked conjugates were assayed for RNase P activity by incubation in the presence of 50 nM radiolabeled pre-tRNA, for intramolecular crosslinks, or alone, for intermolecular crosslinks, in 3 M ammonium acetate, 25 mM magnesium chloride, 40 mM Tris-HCl, pH 8.0, 0.1% SDS. Reactions were incubated at 37 °C for 5–10 min, and the products were resolved on denaturing polyacrylamide gels.

For primer-extension mapping of crosslink sites, RNA was recovered from crosslinking reactions by ethanol precipitation and the crosslinked species were resolved by electrophoresis through 4% polyacrylamide/8 M urea gels. RNAs were visualized by staining with ethidium bromide and excised from the gel. The various crosslinked species as well as the uncrosslinked RNA were eluted as described above. Crosslinked nucleotides were determined by primer extension of the crosslinked RNA as described previously (Burgin & Pace, 1990).

Structure modeling

Model helices and structures were generated using MC-SYM (Major et al., 1994). Manual positioning and structure refinement were performed using Insight II (Biosym). Refinement was performed by steepest-decent energy minimization using the amber forcefield. Molecular graphics were generated using RIBBONS (Carson, 1987). Coordinates are available by request from meh2@pop.cwru.edu.

NOTE ADDED IN PROOF

Additional evidence for a P1-P9 interaction from phylogenetic sequence comparisons is provided by Massire et al. in this issue.

ACKNOWLEDGMENTS

We thank Stephen Harvey and Tom Easterwood for expert help and advice on computer modeling, as well as access to model-structure coordinates. We thank Brandt Burgess for assistance with analysis of crosslinked RNA mobilities. We also gratefully acknowledge our colleagues in the Pace laboratory for help and advice during the course of this work. This work was supported by NIH grant GM34527 (N.R.P.) and NIH Postdoctoral Fellowship GM15979 (M.E.H.).

Received November 13, 1996; returned for revision January 15, 1997; revised manuscript received March 17, 1997

REFERENCES

Baer MF, Reilly RM, McCorkle GM, Hai TY, Altman S, RajBhandary UL. 1988. The recognition by RNase P of precursor tRNAs. *J Biol Chem 263*:2344–2351.

Brimacombe R. 1995. The structure of ribosomal RNA: A three-dimensional jigsaw puzzle. *Eur J Biochem 230*:365–383.

Brown JW, Haas ES, Gilbert DG, Pace NR. 1994. The ribonuclease P database. *Nucleic Acids Res 22*:3660–3662.

Brown JW, Nolan JM, Haas ES, Rubio MAT, Major F, Pace NR. 1996. Comparative analysis of ribonuclease P RNA using gene sequences from natural microbial populations reveals tertiary structure elements. *Proc Natl Acad Sci USA 91*:3001–3006.

Burgin AB, Pace NR. 1990. Mapping the active site of ribonuclease P RNA using a substrate containing a photoaffinity agent. *EMBO J 9*:4111–4118.

Carson M. 1987. Ribbon models of macromolecules. *J Mol Graph 5*:103–106.

Cate JH, Gooding AR, Podell E, Zhou K, Golden BL, Kundrot CE, Cech TR, Doudna JA. 1996. Crystal structure of a group I ribozyme domain: Principles of RNA packing. *Science 273*:1678–1685.

Cech TR. 1993. Structure and mechanism of the large catalytic RNAs: Group I and group II introns and ribonuclease P. In: Atkins RFG, Gesteland JF, eds. *The RNA world*. Cold Spring Harbor, New York: Cold Spring Harbor Laboratory Press. pp 239–269.

Cherayil B, Krupp G, Schuchert P, Char S, Söll D. 1987. The RNA components of *Schizosaccharomyces pombe* RNase P are essential for cell viability. *Gene 60*:157–161.

Costa M, Michel F. 1995. Frequent use of the same tertiary motif by self-folding RNAs. *EMBO J 14*:1276–1285.

Denman R, Colgen J, Nurse K, Ofengand J. 1988. Crosslinking of the anticodon of P site bound tRNA to C-1400 of *E. coli* 16S RNA does not require the participation of the 50S subunit. *Nucleic Acids Res 16*:165–178.

Easterwood T, Harvey SC. 1997. Ribonuclease P RNA: Models of the 15/16 bulge from *Escherichia coli* and the P15 stem loop of *Bacillus subtilis*. *RNA 3*:577–585.

Guerrier-Takada C, Gardiner K, Marsh T, Pace N, Altman S. 1983. The RNA moiety of ribonuclease P is the catalytic subunit of the enzyme. *Cell 35*:849–857.

Haas ES, Banta AB, Harris JK, Pace NR, Brown JW. 1997. Structure and evolution of ribonuclease P RNA in gram-positive bacteria. *Nucleic Acids Res 24*:4775–4782.

Harris ME, Nolan JM, Malhotra A, Brown JW, Harvey SC, Pace NR. 1994. Use of photoaffinity crosslinking and molecular modeling to analyze the global architecture of ribonuclease P RNA. *EMBO J 13*:3953–3963.

Harris ME, Pace NR. 1995. Identification of phosphates involved in catalysis by the ribozyme RNase P RNA. *RNA 1*:210–218.

James BD, Olsen GJ, Liu J, Pace NR. 1988. The secondary structure of ribonuclease P RNA, the catalytic element of a ribonucleoprotein enzyme. *Cell 52*:19–26.

Kirsebom LA, Svärd SG. 1993. Identification of a region within M1 RNA of *Escherichia coli* RNase P important for the location of the cleavage site on a wild-type tRNA precursor. *J Mol Biol 231*:594–604.

Kirsebom LA, Svärd SG. 1994. Base pairing between *Escherichia coli* RNase P RNA and its substrate. *EMBO J 13*:4870–4876.

LaGrandeur TE, Darr SC, Haas ES, Pace NR. 1993. Characterization of the RNase P RNA of *Sulfolobus acidocaldarius*. *J Bacteriol 175*:5043–5048.

LaGrandeur TE, Hüttenhofer A, Noller HF, Pace NR. 1994. Phylogenetic comparative chemical footprint analysis of the interaction between ribonuclease p RNA and tRNA. *EMBO J 13*:3945–3952.

Lane DJ, Field KG, Olsen GJ, Pace NR. 1988. Reverse transcriptase sequencing of ribosomal RNA for phylogenetic analysis. *Methods Enzymol 167*:138–44.

Malhotra A, Harvey, SC. 1994. A quantitative model of the *Escherichia coli* 16S RNA in the 30S ribosomal subunit. *J Mol Biol 240*: 308–340.

Michel F, Westhof E. 1990. Modelling of the three-dimensional architecture of group I catalytic introns based on comparative sequence analysis. *J Mol Biol 216*:585–610.

Milligan JF, Uhlenbeck OC. 1989. Synthesis of small RNAs using T7 RNA polymerase. *Methods Enzymol 164*:51–62.

Mitchell P, Stade K, Osswald M, Brimacombe R. 1993. Site-directed cross-linking studies on the *E. coli* tRNA-ribosome complex: Determination of sites labelled with an aromatic azide attached to the variable loop or aminoacyl group of tRNA. *Nucleic Acids Res 21*:887–896.

Nolan JM, Burke DH, Pace NR. 1993. Circularly permuted tRNAs as specific photoaffinity probes of ribonuclease P RNA structure. *Science 261*:762–765.

Oh BK, Pace NR. 1994. Interaction of the 3′-end of tRNA with ribonuclease P RNA. *Nucleic Acids Res 22*:4087–4094.

Pace NR, Brown JW. 1995. Evolutionary perspective on the structure and function of ribonuclease P, a ribozyme. *J Bacteriol 177*:1919–1928.

Pan T. 1995. Higher order folding and domain analysis of the ribozyme from *Bacillus subtilis* ribonuclease P. *Biochemistry 34*:902–909.

Pan T, Loria A, Zhong K. 1995. Probing of tertiary interactions in RNA: 2′-Hydroxyl-base contacts between the RNase P RNA and pre-tRNA. *Proc Natl Acad Sci USA 92*:12510–12514.

Pley HW, Flaherty KM, McKay DB. 1994. Three-dimensional structure of a hammerhead ribozyme. *Nature 372*:68–74.

Reich C, Olsen GJ, Pace B, Pace NR. 1988. Role of the protein moiety of ribonuclease P, a ribonucleoprotein enzyme. *Science 239*:178–181.

Schlegl J, Hardt WD, Erdmann VA, Hartmann RK. 1994. Contribution of structural elements to *Thermus thermophilus* ribonuclease P RNA function. *EMBO J 13*:4863–4869.

Schuster GB, Platz MS. 1992. Photochemistry of phenyl azide. *Adv Photochem 17*:69–143.

Scott WG, Finch JT, Klug A. 1996. The crystal structure of an all-RNA hammerhead ribozyme: A proposed mechanism for RNA catalytic cleavage. *Cell 81*:991–1002.

Shiraishi H, Shimura Y. 1986. Mutations affecting two distinct functions of the RNA component of RNase P. *EMBO J 5*:3673–3679.

Smith D, Burgin AB, Haas ES, Pace NR. 1992. Influence of metal ions on the ribonuclease P reaction. Distinguishing substrate binding from catalysis. *J Biol Chem 267*:2429–2436.

Stade K, Rines S, Bochkariov D, Brimacombe R. 1994. Contacts between the growing peptide chain and the 23S RNA in the 50S ribosomal subunit. *Nucleic Acids Res 22*:1394–1399.

Stern S, Weiser B, Noller HF. 1988. Model for the three-dimensional folding of 16S ribosomal RNA. *J Mol Biol 204*:448–481.

Tallsjö A, Kirsebom LA. 1993. Product release is a rate-limiting step during cleavage by the catalytic RNA subunit of *Escherichia coli* RNase P. *Nucleic Acids Res 21*:51–57.

Westhof E, Wesolowski D, Altman S. 1996. Mapping in three dimensions of regions in a catalytic RNA protected from attack by an Fe(II)-EDTA reagent. *J Mol Biol 258*:600–613.